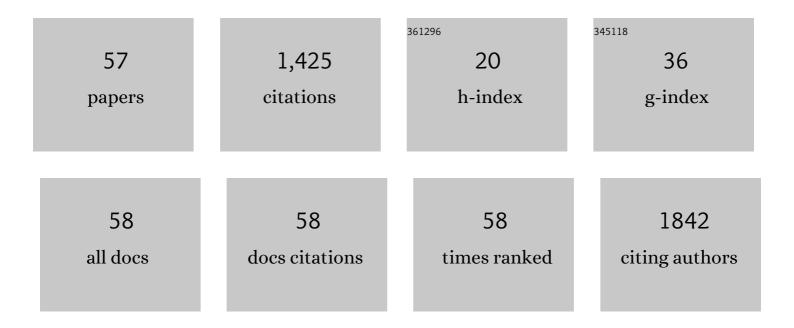
Cheng-Chien Liu

List of Publications by Year in descending order

Source: https://exaly.com/author-pdf/4825152/publications.pdf Version: 2024-02-01



#	Article	IF	CITATIONS
1	Impacts of the Chi-Chi earthquake on subsequent rainfall-induced landslides in central Taiwan. Engineering Geology, 2006, 86, 87-101.	2.9	234
2	lce shelf disintegration by plate bending and hydro-fracture: Satellite observations and model results of the 2008 Wilkins ice shelf break-ups. Earth and Planetary Science Letters, 2009, 280, 51-60.	1.8	226
3	Automatic extraction of ground control regions and orthorectification of remote sensing imagery. Optics Express, 2009, 17, 7970.	1.7	93
4	Innovative landslide susceptibility mapping supported by geomorphon and geographical detector methods. Landslides, 2018, 15, 465-474.	2.7	80
5	Processing of FORMOSAT-2 Daily Revisit Imagery for Site Surveillance. IEEE Transactions on Geoscience and Remote Sensing, 2006, 44, 3206-3214.	2.7	53
6	Image processing of FORMOSATâ€2 data for monitoring the South Asia tsunami. International Journal of Remote Sensing, 2007, 28, 3093-3111.	1.3	43
7	Emissions Inventory for Rice Straw Open Burning in Taiwan Based on Burned Area Classification and Mapping Using Formosat-2 Satellite Imagery. Aerosol and Air Quality Research, 2013, 13, 474-487.	0.9	41
8	Clouds Classification from Sentinel-2 Imagery with Deep Residual Learning and Semantic Image Segmentation. Remote Sensing, 2019, 11, 119.	1.8	39
9	A Multi-Sensor Approach to Examining the Distribution of Total Suspended Matter (TSM) in the Albemarle-Pamlico Estuarine System, NC, USA. Remote Sensing, 2011, 3, 962-974.	1.8	38
10	Flood Prevention and Emergency Response System Powered by Google Earth Engine. Remote Sensing, 2018, 10, 1283.	1.8	35
11	Rapid Response to a Typhoon-Induced Flood with an SAR-Derived Map of Inundated Areas: Case Study and Validation. Remote Sensing, 2015, 7, 11954-11973.	1.8	31
12	Fast and accurate model of underwater scalar irradiance. Applied Optics, 2002, 41, 4962.	2.1	29
13	Rapidly responding to landslides and debris flow events using a low-cost unmanned aerial vehicle. Journal of Applied Remote Sensing, 2015, 9, 096016.	0.6	27
14	A New Approach Using AHP to Generate Landslide Susceptibility Maps in the Chen-Yu-Lan Watershed, Taiwan. Sensors, 2019, 19, 505.	2.1	27
15	Vicarious Calibration of the Formosat-2 Remote Sensing Instrument. IEEE Transactions on Geoscience and Remote Sensing, 2010, 48, 2162-2169.	2.7	25
16	Surface Heat Balance Analysis of Tainan City on March 6, 2001 Using ASTER and Formosat-2 Data. Sensors, 2008, 8, 6026-6044.	2.1	23
17	Integrating semianalytical and genetic algorithms to retrieve the constituents of water bodies from remote sensing of ocean color. Optics Express, 2007, 15, 252.	1.7	22
18	Illumination and turbidity effects on observing faceted bottom elements with uniform Lambertian albedos. Limnology and Oceanography, 2003, 48, 355-363.	1.6	21

CHENG-CHIEN LIU

#	Article	IF	CITATIONS
19	Optical model for use in oceanic ecosystem models. Applied Optics, 1999, 38, 4475.	2.1	20
20	Preparing a landslide and shadow inventory map from high-spatial-resolution imagery facilitated by an expert system. Journal of Applied Remote Sensing, 2015, 9, 096080.	0.6	20
21	Supporting the annual international black-faced spoonbill census with a low-cost unmanned aerial vehicle. Ecological Informatics, 2015, 30, 170-178.	2.3	20
22	Controls of preferential orientation of earthquake―and rainfallâ€ŧriggered landslides in Taiwan's orogenic mountain belt. Earth Surface Processes and Landforms, 2019, 44, 1661-1674.	1.2	20
23	Terrain attributes of earthquake―and rainstormâ€induced landslides in orogenic mountain Belt, Taiwan. Earth Surface Processes and Landforms, 2017, 42, 1549-1559.	1.2	18
24	Change detection of gravel mining on riverbeds from the multiâ€ŧemporal and highâ€spatialâ€ŧesolution formosatâ€2 imagery. River Research and Applications, 2009, 25, 1136-1152.	0.7	16
25	Monitoring the dynamics of ice shelf margins in Polar Regions with high-spatial- and high-temporal-resolution space-borne optical imagery. Cold Regions Science and Technology, 2009, 55, 14-22.	1.6	16
26	Spectrum matching method for estimating the chlorophyll- <i>a</i> concentration, CDOM ratio, and backscatter fraction from remote sensing of ocean color. Canadian Journal of Remote Sensing, 2008, 34, 343-355.	1.1	15
27	Classification of non-vegetated areas using Formosat-2 high spatiotemporal imagery: the case of Tseng-Wen Reservoir catchment area (Taiwan). International Journal of Remote Sensing, 2011, 32, 8519-8540.	1.3	15
28	Monitoring reservoir water quality with Formosat-2 high spatiotemporal imagery. Journal of Environmental Monitoring, 2009, 11, 1982.	2.1	14
29	Prediction of ocean colour: Monte Carlo simulation applied to a virtual ecosystem based on the Lagrangian Ensemble method. International Journal of Remote Sensing, 2004, 25, 921-936.	1.3	12
30	Estimating the underwater light field from remote sensing of ocean color. Journal of Oceanography, 2006, 62, 235-248.	0.7	12
31	Rapid locating of fire points from Formosat-2 high spatial resolution imagery: example of the 2007 California wildfire. International Journal of Wildland Fire, 2009, 18, 415.	1.0	12
32	Assessment of forest restoration with multitemporal remote sensing imagery. Scientific Reports, 2019, 9, 7279.	1.6	10
33	Spatiotemporal variation of Gaoping River plume observed by Formosat-2 high resolution imagery. Journal of Marine Systems, 2014, 132, 28-37.	0.9	9
34	Using satellite observations of ocean color to categorize the dispersal patterns of river-borne substances in the Gaoping (Kaoping) River, Shelf and Canyon system. Journal of Marine Systems, 2009, 76, 496-510.	0.9	8
35	Application of multi-scale remote sensing imagery to detection and hazard analysis. Natural Hazards, 2013, 65, 2241-2252.	1.6	8
36	A new region-based preparatory factor for landslide susceptibility models: the total flux. Landslides, 2016, 13, 1049-1056.	2.7	8

CHENG-CHIEN LIU

#	Article	IF	CITATIONS
37	Cross Calibration of Formosat-2 Remote Sensing Instrument (RSI) Using Terra Advanced Spaceborne Thermal Emission and Reflection Radiometer (ASTER). IEEE Transactions on Geoscience and Remote Sensing, 2012, 50, 4821-4831.	2.7	7
38	Comparison of surface heat balance in three cities in Taiwan using Terra ASTER and Formosat-2 RSI data. International Journal of Applied Earth Observation and Geoinformation, 2012, 18, 263-273.	1.4	7
39	Development and evaluation of a genetic algorithm-based ocean color inversion model for simultaneously retrieving optical properties and bottom types in coral reef regions. Applied Optics, 2014, 53, 605.	0.9	7
40	Identification of inventory-based susceptibility models for assessing landslide probability: a case study of the Gaoping River Basin, Taiwan. Geomatics, Natural Hazards and Risk, 2017, 8, 1730-1751.	2.0	7
41	First space-borne high-spatial-resolution optical imagery of the Antarctic from Formosat-2. Antarctic Science, 2008, 20, 605-606.	0.5	6
42	High quality DEM generation from PCIAS. , 2012, , .		6
43	Mapping Pure Mangrove Patches in Small Corridors and Sandbanks Using Airborne Hyperspectral Imagery. Remote Sensing, 2019, 11, 592.	1.8	6
44	Fast and accurate model of underwater scalar irradiance for stratified Case 2 waters. Optics Express, 2006, 14, 1703.	1.7	4
45	Emergency responses to natural disasters using Formosat-2 high-spatiotemporal-resolution imagery: forest fires. Natural Hazards, 2013, 66, 1037-1057.	1.6	4
46	Influences of the Shadow Inventory on a Landslide Susceptibility Model. ISPRS International Journal of Geo-Information, 2018, 7, 374.	1.4	4
47	Instability Index Derived from a Landslide Inventory for Watershed Stability Assessment and Mapping. ISPRS International Journal of Geo-Information, 2019, 8, 145.	1.4	4
48	Spatiotemporal Variation of Cold Eddies in the Upwelling Zone off Northeastern Taiwan Revealed by the Geostationary Satellite Imagery of Ocean Color and Sea Surface Temperature. Sustainability, 2019, 11, 6979.	1.6	4
49	Investigating Sediment Dynamics in a Landslide-Dominated Catchment by Modeling Landslide Area and Fluvial Sediment Export. Water (Switzerland), 2020, 12, 2907.	1.2	4
50	Responding to natural disasters with satellite imagery. SPIE Newsroom, 0, , .	0.1	4
51	Flow Induced by a Pair of Line Vortices Moving against a Circular Cylinder. Journal of the Physical Society of Japan, 1995, 64, 1557-1578.	0.7	3
52	Near Real-Time Browsable Landsat-8 Imagery. Remote Sensing, 2017, 9, 79.	1.8	3
53	Adaptive Contrast Enhancement of Optical Imagery Based on Level of Detail (LOD). Remote Sensing, 2020, 12, 1555.	1.8	1
54	Examining Material Transport in Dynamic Coastal Environments: An Integrated Approach Using Field Data, Remote Sensing and Numerical Modeling. Coastal Research Library, 2014, , 333-364.	0.2	1

#	Article	IF	CITATIONS
55	A spectrum matching method for estimating the inherent optical properties from remote sensing of ocean color. , 2003, , .		0
56	Monitoring the illegal quarry mining of gravel on the riverbed using daily revisit FORMOSAT-2 imagery. , 0, , .		0
57	Deriving Ocean Surface Currents: A method using Geostationary Ocean Color Imager hourly data. IEEE Geoscience and Remote Sensing Magazine, 2021, 9, 138-156.	4.9	0